This document is downloaded from DR-NTU (https://dr.ntu.edu.sg)
Nanyang Technological University, Singapore.

Molybdenum disulfide (MoS_2) as a broadband saturable absorber for ultra-fast photonics

Zhang, H; Lu, S B; Zheng, J; Du, J; Wen, S C; Tang, D Y; Loh, K P

2014

Zhang, H., Lu, S. B., Zheng, J., Du, J., Wen, S. C., Tang, D. Y., et al. (2014). Molybdenum disulfide (MoS_2) as a broadband saturable absorber for ultra-fast photonics. Optics Express, 22(6), 7249-7260.

https://hdl.handle.net/10356/104128

https://doi.org/10.1364/OE.22.007249

© 2014 Optical Society of America. This paper was published in Optics Express and is made available as an electronic reprint (preprint) with permission of Optical Society of America. The paper can be found at the following official DOI: http://dx.doi.org/10.1364/OE.22.007249. One print or electronic copy may be made for personal use only. Systematic or multiple reproduction, distribution to multiple locations via electronic or other means, duplication of any material in this paper for a fee or for commercial purposes, or modification of the content of the paper is prohibited and is subject to penalties under law.

Downloaded on 26 Aug 2022 03:31:33 SGT

Molybdenum disulfide (MoS_2) as a broadband saturable absorber for ultra-fast photonics

H. Zhang,[1,3,5] S. B. Lu,[2,5] J. Zheng,[3] J. Du,[2] S. C. Wen,[2] D. Y. Tang,[4] and K. P. Loh[3,*]

[1]*Key Laboratory of Optoelectronic Devices and Systems of Ministry of Education and Guangdong Province, Shenzhen University, Shenzhen 518060, China*
[2]*Key Laboratory for Micro-Nano Optoelectronic Devices of Ministry of Education, College of Physics and Microelectronic Science, Hunan University, Changsha 410082, China*
[3]*Department of Chemistry and Graphene Research Centre, National University of Singapore, 3 Science Drive 3, Singapore 117543, Singapore*
[4]*School of Electrical and Electronic Engineering, Nanyang Technological University, Singapore 639798, Singapore*
[5]*Equal contributions*
[*]*chmlohkp@nus.edu.sg*

Abstract: The nonlinear optical property of few-layered MoS_2 nanoplatelets synthesized by the hydrothermal exfoliation method was investigated from the visible to the near-infrared band using lasers. Both open-aperture Z-scan and balanced-detector measurement techniques were used to demonstrate the broadband saturable absorption property of few-layered MoS_2. To explore its potential applications in ultrafast photonics, we fabricated a passive mode locker for ytterbium-doped fibre laser by depositing few-layered MoS_2 onto the end facet of optical fiber by means of an optical trapping approach. Our laser experiment shows that few-layer MoS_2-based mode locker allows for the generation of stable mode-locked laser pulse, centered at 1054.3 nm, with a 3-dB spectral bandwidth of 2.7 nm and a pulse duration of 800 ps. Our finding suggests that few-layered MoS_2 nanoplatelets can be useful nonlinear optical material for laser photonics devices, such as passive laser mode locker, Q-switcher, optical limiter, optical switcher and so on.

©2014 Optical Society of America

OCIS codes: (160.4330) Nonlinear optical materials; (160.4236) Nanomaterials; (190.7110) Ultrafast nonlinear optics.

References and links

1. K. S. Novoselov, A. K. Geim, S. V. Morozov, D. Jiang, Y. Zhang, S. V. Dubonos, I. V. Grigorieva, and A. A. Firsov, "Electric field effect in atomically thin carbon films," Science **306**(5696), 666–669 (2004).
2. A. H. Castro Neto, F. Guinea, N. M. R. Peres, K. S. Novoselov, and A. K. Geim, "The electronic properties of graphene," Rev. Mod. Phys. **81**(1), 109–162 (2009).
3. F. Bonaccorso, Z. Sun, T. Hasan, and A. C. Ferrari, "Graphene photonics and optoelectronics," Nat. Photonics **4**(9), 611–622 (2010).
4. S. Yamashita, "A tutorial on nonlinear photonic applications of carbon nanotube and graphene," J. Lightwave Technol. **30**(4), 427–447 (2012).
5. A. H. Castro Neto and K. Novoselov, "Two dimensional crystals: beyond graphene," Mater. Express **1**(1), 10–17 (2011).
6. M. S. Xu, T. Liang, M. Shi, and H. Z. Chen, "Graphene-like two-dimensional materials," Chem. Rev. **113**(5), 3766–3798 (2013).
7. K. Wang, J. Wang, J. Fan, M. Lotya, A. O'Neill, D. Fox, Y. Feng, X. Zhang, B. Jiang, Q. Zhao, H. Zhang, J. N. Coleman, L. Zhang, and W. J. Blau, "Ultrafast saturable absorption of two-dimensional MoS_2 nanosheets," ACS Nano **7**(10), 9260–9267 (2013).
8. L. Britnell, R. M. Ribeiro, A. Eckmann, R. Jalil, B. D. Belle, A. Mishchenko, Y.-J. Kim, R. V. Gorbachev, T. Georgiou, S. V. Morozov, A. N. Grigorenko, A. K. Geim, C. Casiraghi, A. H. Castro Neto, and K. S. Novoselov, "Strong light-matter interactions in heterostructures of atomically thin films," Science **340**(6138), 1311–1314 (2013).
9. A. Carvalho, R. M. Ribeiro, and A. H. Castro Neto, "Band nesting and the optical response of two-dimensional semiconducting transition metal dichalcogenides," Phys. Rev. B **88**(11), 115205 (2013).

#205894 - $15.00 USD Received 3 Feb 2014; revised 10 Mar 2014; accepted 12 Mar 2014; published 20 Mar 2014

10. Q. H. Wang, K. Kalantar-Zadeh, A. Kis, J. N. Coleman, and M. S. Strano, "Electronics and optoelectronics of two-dimensional transition metal dichalcogenides," Nat. Nanotechnol. **7**(11), 699–712 (2012).
11. C. Ataca, H. Şahin, and S. Ciraci, "Stable, single-layer MX2 transition-metal oxides and dichalcogenides in a honeycomb-like structure," J. Phys. Chem. C **116**(16), 8983–8999 (2012).
12. K. F. Mak, C. Lee, J. Hone, J. Shan, and T. F. Heinz, "Atomically thin MoS_2: a new direct-gap semiconductor," Phys. Rev. Lett. **105**(13), 136805 (2010).
13. J. N. Coleman, M. Lotya, A. O'Neill, S. D. Bergin, P. J. King, U. Khan, K. Young, A. Gaucher, S. De, R. J. Smith, I. V. Shvets, S. K. Arora, G. Stanton, H. Y. Kim, K. Lee, G. T. Kim, G. S. Duesberg, T. Hallam, J. J. Boland, J. J. Wang, J. F. Donegan, J. C. Grunlan, G. Moriarty, A. Shmeliov, R. J. Nicholls, J. M. Perkins, E. M. Grieveson, K. Theuwissen, D. W. McComb, P. D. Nellist, and V. Nicolosi, "Two-dimensional nanosheets produced by liquid exfoliation of layered materials," Science **331**(6017), 568–571 (2011).
14. Q. L. Bao, H. Zhang, Y. Wang, Z. Ni, Y. Yan, Z. X. Shen, K. P. Loh, and D. Y. Tang, "Atomic-layer graphene as a saturable absorber for ultrafast pulsed lasers," Adv. Funct. Mater. **19**(19), 3077–3083 (2009).
15. H. Zhang, D. Y. Tang, L. M. Zhao, Q. L. Bao, and K. P. Loh, "Large energy mode locking of an erbium-doped fiber laser with atomic layer graphene," Opt. Express **17**(20), 17630–17635 (2009).
16. Z. Sun, T. Hasan, F. Torrisi, D. Popa, G. Privitera, F. Wang, F. Bonaccorso, D. M. Basko, and A. C. Ferrari, "Graphene mode-locked ultrafast laser," ACS Nano **4**(2), 803–810 (2010).
17. Y. Song, S. Jang, W. Han, and M. Bae, "Graphene mode-lockers for fiber lasers functioned with evanescent field interaction," Appl. Phys. Lett. **96**(5), 051122 (2010).
18. F. Bonaccorso and Z. Sun, "Solution processing of graphene, topological insulators and other 2d crystals for ultrafast photonics," Opt. Mater. Express **4**(1), 63–78 (2014).
19. J. Zheng, H. Zhang, S. Dong, Y. Liu, C. T. Nai, H. S. Shin, H. Y. Jeong, B. Liu, and K. P. Loh, "High yield exfoliation of two-dimensional chalcogenides using sodium naphthalenide," Nat. Commun. **5**, 2995 (2014).
20. L. Ren, X. Qi, Y. Liu, G. Hao, Z. Huang, X. Zou, L. Yang, J. Li, and J. Zhong, "Large-scale production of ultrathin topological insulator bismuth telluride nanosheets by a hydrothermal intercalation and exfoliation route," J. Mater. Chem. **22**(11), 4921–4926 (2012).
21. A. Splendiani, L. Sun, Y. Zhang, T. Li, J. Kim, C. Y. Chim, G. Galli, and F. Wang, "Emerging photoluminescence in monolayer MoS_2.," Nano Lett. **10**(4), 1271–1275 (2010).
22. P. Tonndorf, R. Schmidt, P. Böttger, X. Zhang, J. Börner, A. Liebig, M. Albrecht, C. Kloc, O. Gordan, D. R. T. Zahn, S. Michaelis de Vasconcellos, and R. Bratschitsch, "Photoluminescence emission and Raman response of monolayer MoS_2, $MoSe_2$, and WSe_2," Opt. Express **21**(4), 4908–4916 (2013).
23. H. Li, Q. Zhang, C. C. R. Yap, B. K. Tay, T. H. T. Edwin, A. Olivier, and D. Baillargeat, "From bulk to monolayer MoS2: evolution of Raman scattering," Adv. Funct. Mater. **22**(7), 1385–1390 (2012).
24. H. Zhang, S. Virally, Q. Bao, L. K. Ping, S. Massar, N. Godbout, and P. Kockaert, "Z-scan measurement of the nonlinear refractive index of graphene," Opt. Lett. **37**(11), 1856–1858 (2012).
25. R. A. Ganeev, A. I. Ryasnyansky, N. Ishizawa, M. Baba, M. Suzuki, M. Turu, S. Sakakibara, and H. Kuroda, "Two- and three-photon absorption in CS_2," Opt. Commun. **231**(1–6), 431–436 (2004).
26. K. P. Loh, H. Zhang, W. Z. Chen, and W. Ji, "Templated deposition of MoS_2 nanotubules using single source precursor and studies of their optical limiting properties," J. Phys. Chem. B **110**(3), 1235–1239 (2006).
27. J. Wang, Y. Hernandez, M. Lotya, J. N. Coleman, and W. J. Blau, "Broadband nonlinear optical response of graphene dispersions," Adv. Mater. **21**(23), 2430–2435 (2009).
28. E. Garmire, "Resonant optical nonlinearities in semiconductors," IEEE J. Sel. Top. Quantum Electron. **6**(6), 1094–1110 (2000).
29. P. Grelu and N. Akhmediev, "Dissipative solitons for mode-locked lasers," Nat. Photonics **6**(2), 84–92 (2012).
30. K. Kieu and F. W. Wise, "All-fiber normal-dispersion femtosecond laser," Opt. Express **16**(15), 11453–11458 (2008).
31. H. Zhang, D. Tang, R. J. Knize, L. Zhao, Q. Bao, and K. P. Loh, "Graphene mode-locked, wavelength-tunable, dissipative soliton fibre laser," Appl. Phys. Lett. **96**(11), 111112 (2010).
32. G. Sobon, J. Sotor, J. Jagiello, R. Kozinski, Ma. Zdrojek, M. Holdynski, P. Paletko, J. Boguslawski, L. Lipinska, and K. M. Abramski, "Graphene oxide vs. reduced graphene oxide as saturable absorbers for Er-doped passively mode-locked fibre laser," Opt. Express **20**(17), 19463–19473 (2012).
33. A. Martinez, K. Fuse, B. Xu, and S. Yamashita, "Optical deposition of graphene and carbon nanotubes in a fiber ferrule for passive mode-locked lasing," Opt. Express **18**(22), 23054–23061 (2010).
34. P. L. Huang, S. C. Lin, C. Y. Yeh, H. H. Kuo, S. H. Huang, G. R. Lin, L. J. Li, C. Y. Su, and W. H. Cheng, "Stable mode-locked fiber laser based on CVD fabricated graphene saturable absorber," Opt. Express **20**(3), 2460–2465 (2012).

1. Introduction

Since graphene was first isolated from graphite, its electronic and optical properties have been studied extensively and applied in various fields [1–4]. The success of graphene applications motivates the exploration of other graphene-like two-dimensional (2D) materials in which strong intra-layer covalent bonding and weak inter-layer van der Waals forces exist [5, 6]. But the photonic applications of 2D crystals remain much less actively investigated. Although

saturable absorption in molybdenum disulfide (MoS_2) has been reported [7], ultrafast pulse generation has yet to be demonstrated. Single-layer transition metal dichalcogenides (TMDs) display surprisingly strong bulk-like photon absorption and exciton generation owing to Van Hove singularities [8] and possibly band nesting [9]. MoS_2 is a typical TMD, in which hexagonal layers of molybdenum atoms are sandwiched between two layers of chalcogen atoms (S) [10, 11]. As with graphene, layered materials must be exfoliated into thin sheets to reveal their extraordinary properties. The optical properties of MoS_2 show interesting layer dependence. The excitonic transition at the *K* point in the Brillouin zone of MoS_2 remains direct regardless of layer thickness, whereas the indirect band-gap energy between the Γ and *K* points increases as layer thickness decreases. The indirect-to-direct transition occurs as MoS_2 is exfoliated into monolayer sheets, resulting in the dramatic enhancement of photoluminescence [12, 13]. This exotic optical-electrical property makes few-layered MoS_2 a potential optical material for use in optoelectronics.

Optical materials with different nonlinear optical responses (optical limiting and saturable absorption) are widely used for photonic devices such as optical limiters, mode-lockers, and Q-switchers [14, 15]. Graphene has been shown to exhibit broadband optical saturable absorption property and has been applied successfully in passive mode locking or Q-switching of both fibre and solid-state lasers [14–17]. Very recently, Wang *et al.* reported that MoS_2 dispersions with large populations of single and few layers produced by liquid-phase exfoliation exhibit significant saturable absorption under femtosecond laser excitation at 800 nm and show better saturable absorption response than does graphene [7]. The potential photonics applications of solution-processed 2-dimenional layered materials, such as MoS_2, WS_2, Bi_2Se_3, and Bi_2Te_3, had been summarized by Bonaccorso *et al*. [18]. Recently, we demonstrated the high-yield exfoliation of 2D chalcogenides by reduction with sodium naphthalenide; the solution-dispersible flakes can be easily manipulated and provide an opportunity to study the ultrafast photonics of 2D chalcogenide films [19].

In this contribution, we experimentally confirm that MoS_2 shows broadband saturable absorption response from the visible to the near-infrared band and demonstrate the first ultrafast photonics application of MoS_2 saturable absorber for passive laser mode-locking operation. To take advantage of its near-infrared saturable absorption property, we have developed a MoS_2-based optical fibre saturable absorber device with operation wavelength suitable for an ytterbium-doped fibre laser and experimentally generated nanosecond pulses, indicating that the MoS_2 saturable absorber possesses excellent mode-locking ability comparable with other saturable absorbers such as graphene.

2. Experimental preparation and setup

2.1. Preparation of MoS_2 nanoplatelets

Hydrothermal intercalation/exfoliation [13, 20], a convenient and cost-effective approach for the synthesis of MoS_2 flakes applied in this work, is shown schematically in Fig. 1. Typically, MoS_2 bulk crystals (0.1 g, 99.999%, Alfa Aesar) were placed into a 50-mL Teflon-lined autoclave filled with 30 mL ethylene glycol and 0.32 g lithium hydroxide. The autoclave was heated at 200°C for 72 hours to achieve the complete intercalation of MoS_2 through the lithium ions (Li^+) dissolved in the solution. After the Li-ion intercalation, the dispersions in the solution were collected by filtration and rinsed with acetone to eliminate the residual ethylene glycol solution and lithium hydroxide. Colloidal suspensions of MoS_2 nanoplatelets (NPs) were prepared by hydrating the lithiated MoS_2 powder in deionised water. The NPs were filtered through porous polyvinylidene fluoride (0.45-lm nominal pore size) membranes, then dried at 60°C to form MoS_2 NPs membranes. All samples for the material characterization and nonlinear optical measurement were dispersed in isopropyl alcohol with a concentration of 0.5 mg/mL.

#205894 - $15.00 USD Received 3 Feb 2014; revised 10 Mar 2014; accepted 12 Mar 2014; published 20 Mar 2014
(C) 2014 OSA

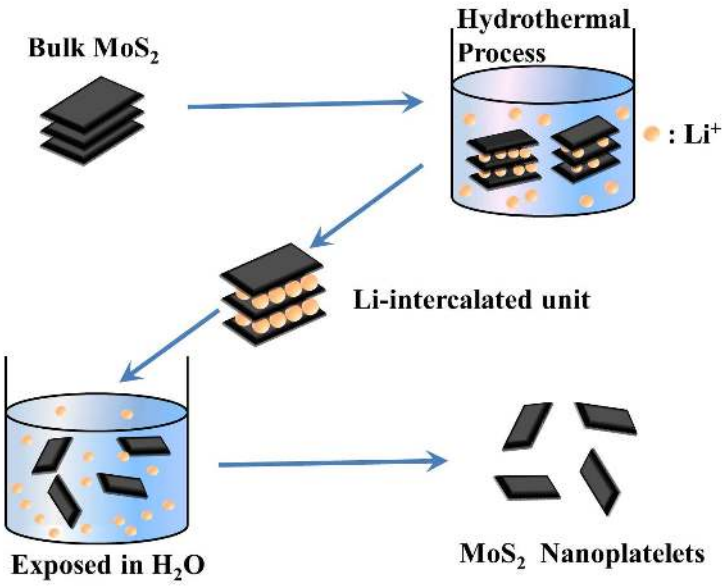

Fig. 1. Schematic diagram of the formation of MoS_2 NPs.

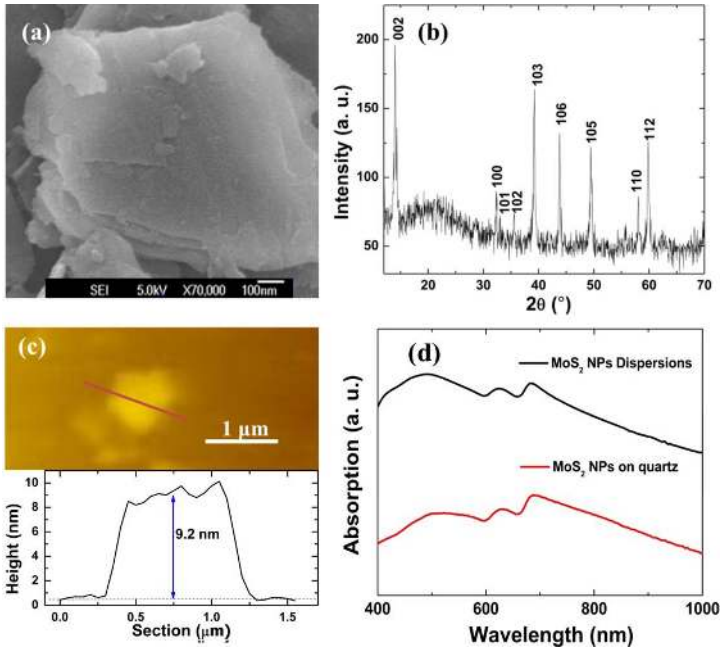

Fig. 2. Characterisation of MoS_2 NPs for Z-scan measurement. (a) Scanning electron microscopy image, (b) XRD diffraction pattern, (c) Atomic force microscopy image and (d) UV-Vis spectra of as-grown MoS_2 NPs.

The characterizations of the MoS_2 NP samples are shown in Fig. 2. Figure 2(a) shows the scanning electron microscopy image of the as-prepared MoS_2 NPs, where the layered structure can be identified at the edge of the NPs. The XRD results of exfoliated MoS_2 NPs in Fig. 2(b) are in good agreement with the hexagonal structure of MoS_2 (PDF Card 04-0880). Atomic force microscopy was used to determine the sample thickness, as shown in Fig. 2(c).

#205894 - $15.00 USD Received 3 Feb 2014; revised 10 Mar 2014; accepted 12 Mar 2014; published 20 Mar 2014
(C) 2014 OSA

The height difference between the quartz substrate and the sample surface is approximately 9.2 nm. Figure 2(d) shows typical UV-Vis spectra of few-layered MoS_2 NPs dispersed in isopropyl alcohol solution and dropped on quarts with a spectrophotometer (Lambda 950). Two peaks around 630 nm and 680 nm arise from the direct-gap transition, which is due to the energy split from valence band and spin-orbit coupling [12, 21]. The broadband absorption in Fig. 2(d) may be related to the presence of both 1T (metallic) and 2H (semiconducting) phases in the as-exfoliated MoS_2 NPs [19]. The 1T phase is known to predominate due to doping by impurities. This means that the saturable absorption properties we study here can be dominated by the metallic phase.

To confirm that the bulk MoS_2 has been successfully exfoliated into few-layer structure, we performed Raman spectroscopy on exfoliated MoS_2 and bulk MoS_2, as shown in Fig. 3. The characteristic peaks of the two samples at 380 and 407 cm^{-1} are assigned to the E^1_{2g} and A_{1g} modes of MoS_2, respectively. The E^1_{2g} mode is correlated with an in-plane motion of Mo and S atoms, while the A_{1g} mode is caused by an out-of-plane vibration of Mo and S [22].Notably, the E^1_{2g} is the shear mode, which is attributed to the relative motion between the adjacent two mono-layers. By comparing the E^1_{2g} mode of bulk MoS_2, one could observe an obvious red shift in the Raman spectra due to the interlayer dependence of the shear modes, which agrees with that of MoS_2 with thicknesses in the range of 1-3 layers [23].

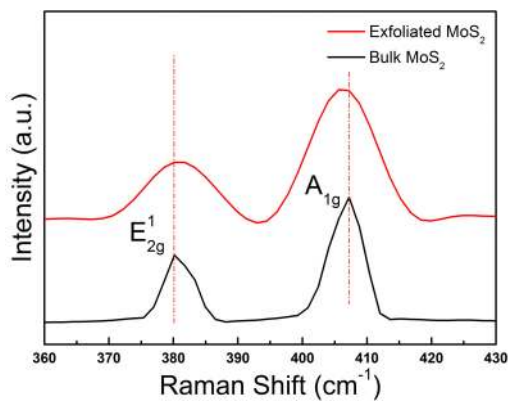

Fig. 3. Raman spectra of the bulk and the exfoliated MoS_2

2.2. Experimental setup

The laser *Z*-scan technique, which was used as an effective tool to measure the nonlinear refractive index of graphene in [24], was used to study the nonlinear optical absorption of the as-prepared MoS_2 NPs. The experimental setup is shown schematically in Fig. 4. The Z-scan measurements were performed by a mode-locked Ti:sapphire oscillator-seeded regenerative amplifier, from which a train of optical pulses (centre wavelength: 800 nm, pulse duration: 100 fs, 3-dB spectral width: 15 nm and repetition rate: 1 kHz) are emitted. A piece of BBO crystal is used to double the frequency of the incident laser pulse at 800 nm through SHG, delivering laser pulses at 400 nm. This technique allows for measurement at different wavelengths.

At first, the MoS_2 dispersion was contained within a 1-mm-thick cuvette for measurement by the incident laser beam (800 nm), which was focused by an objective lens (focal length: 500 mm). The incident beam waist was measured to be about 30 μm by a CCD. By using an optical attenuator, we could adjust the average optical power to below 10 mW, which corresponded to a peak input fluence of 350 mJ/cm^2. The solution cuvette was perpendicularly oriented towards the beam axis and translated along the Z-axis through a linear motorised stage. Computer-controlled power meters were used to simultaneously monitor the referenced and output optical power. To confirm the precision of the experimental

#205894 - $15.00 USD Received 3 Feb 2014; revised 10 Mar 2014; accepted 12 Mar 2014; published 20 Mar 2014
(C) 2014 OSA

setup, the CS_2 solution contained in the cuvette was used for calibration. A typical valley-like *Z*-scan trace could be observed. This allowed the nonlinear optical absorption coefficient of CS_2 to be determined as 4.35×10^{-11} cm/W, which is in good agreement with the 5×10^{-11} cm/W value reported previously [25]. This result demonstrates the reliability of our *Z*-scan measurement platform.

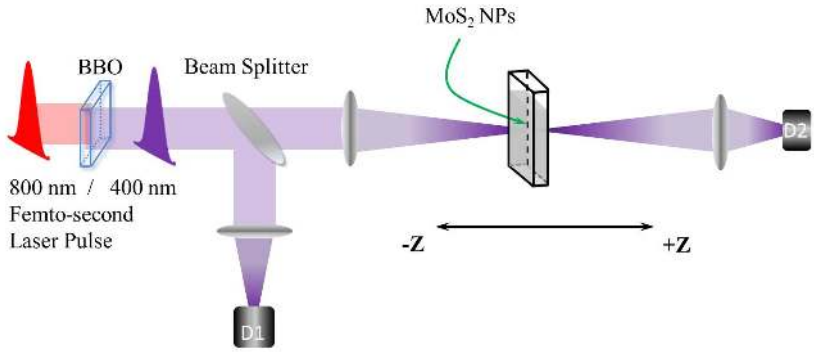

Fig. 4. Schematic diagram of the Z-scan experimental setup.

3. Nonlinear optics results and discussion

The ultrafast nonlinear absorption properties of MoS_2 NPs were investigated by the *Z*-scan technique. Figures 5(a) and 5(b) show the excitation fluence-dependent open-aperture Z-scan measurement results of MoS_2 NP dispersions at both 400 and 800 nm. The sharp and narrow peaks and valleys at the focus point clearly show the characteristics of nonlinear absorption. At the low incident fluence (400 nm), the optical transmittance increases as the sample is translated across the focus point [Fig. 5(a)]. The response is typical of saturable absorption, in which the optical absorbance decreases with the increase of the incident laser flux and becomes saturated above a certain threshold. With the increase of the input fluence, the peaks of the saturable absorption also increase correspondingly. This can be clearly seen from the experimental data at 18 mJ/cm^2 and 35 mJ/cm^2 in Fig. 5(a). However, reverse saturable absorption (RSA) like curve also occurs at a peak intensity of 70 mJ/cm^2. Figure 5(b) shows similar saturable absorption and RSA like behaviour at 800 nm. However, a higher excitation fluence is required to achieve the transition from saturable absorption to RSA at 800 nm than at 400 nm.

The saturable absorption at 400 nm under low incident fluence can be attributed to valence-conduction inter-band transition. The band gaps of few-layered MoS_2 NPs are rather inhomogeneous due to the mixture of the 1T (metallic) and 2H (semiconducting) phases in the as-exfoliated material [19]. As the input fluence increases, electrons in the valence band can be easily pumped to fill the conduction band. Due to the direct band structure and the Pauli blocking principle, the optical absorption saturates at a higher intensity. At higher excitation fluence, nonlinear scattering starts to dominate and leads to the emergence of RSA-like curves, similar to that reported previously [26]. In addition, the origin of the RSA at 800 nm under high input fluence might come from two-photon absorption (TPA) or nonlinear scattering, or a combination of both.

#205894 - $15.00 USD Received 3 Feb 2014; revised 10 Mar 2014; accepted 12 Mar 2014; published 20 Mar 2014
(C) 2014 OSA

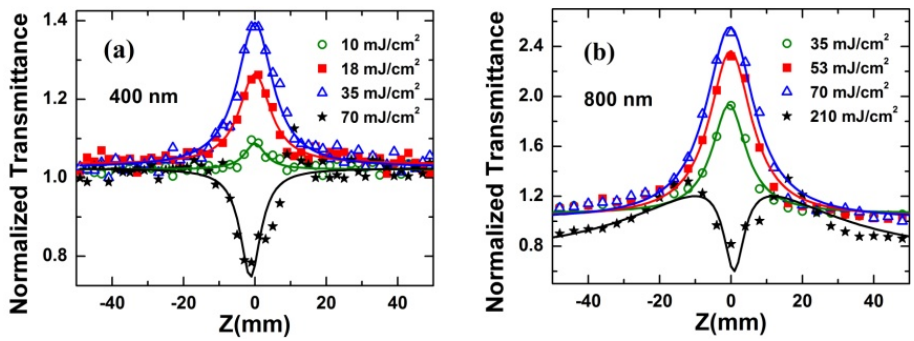

Fig. 5. The open-aperture Z-scan measurements of MoS_2 dispersions in a 1-mm cuvette at (a) 400 nm and (b) 800 nm with different input fluences.

We fitted the experimental Z-scan data with the saturable model that includes both the saturable absorption and TPA effects [27, 28]:

$$\alpha(I) = \frac{\alpha_0}{1 + I / I_s} + \beta I \tag{1}$$

where $\alpha(I)$ is the total absorption coefficient, α_0 is the linear absorption coefficient, I is the input intensity, I_s is the saturable intensity and β is the TPA coefficient. Normally, however, we use the normalized transmittance in the *Z*-scan measurement:

$$T = (1 - \frac{\alpha_0 L}{1 + I / I_s} - \beta I L) / (1 - \alpha_0 L) \tag{2}$$

where L is the sample length. Otherwise, we can use peak intensity I_0 and the diffraction length of the beam Z_0 to determine the intensity:

$$I(z) = \frac{I_0}{(1 + z^2 / z_0^2)}. \tag{3}$$

Thus, we can use the following modified equation to fit the Z-scan experimental data:

$$T = \left[1 - \frac{\alpha_0 L I_s}{I_s + I_0 / (1 + z^2 / z_0^2)} - \beta L I_0 / (1 + z^2 / z_0^2) \right] / (1 - \alpha_0 L). \tag{4}$$

From the fitting curves, we can see that the saturable absorption data fits perfectly; the saturable intensity I_s and modulation depth $\alpha_0 L$ are about 136.1 ± 20 GW/cm^2 and 10% at 400 nm and 279.6 ± 60 GW/cm^2 and 34% at 800 nm, respectively. The TPA β coefficients at the two bands are approximately negligible. The RSA data do not fit very well with the model, possibly due to the multiple origins of the RSA behavior.

#205894 - $15.00 USD Received 3 Feb 2014; revised 10 Mar 2014; accepted 12 Mar 2014; published 20 Mar 2014
(C) 2014 OSA

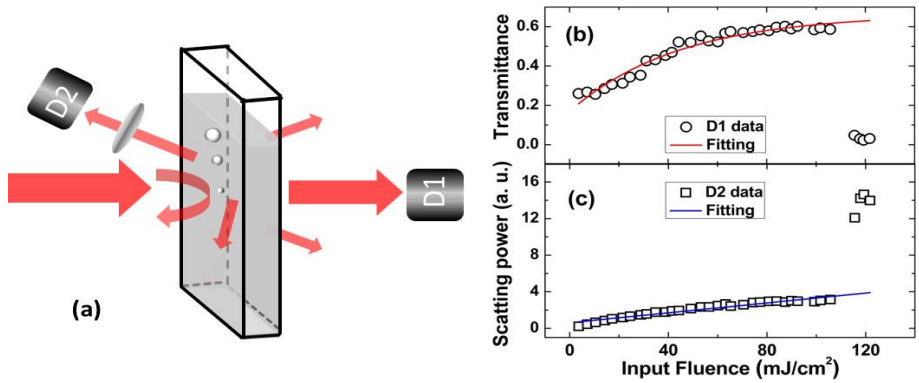

Fig. 6. (a) Schematic diagram of twin-detector measurement; (b) and (c) show the nonlinear transmittance and scattering power, respectively, of MoS_2 dispersions under different input fluences at 800 nm.

To further investigate the nonlinear absorption change at 800 nm, the balanced twin-detector method was used to characterize the nonlinear response of MoS_2 dispersions, as shown in Fig. 6(a). A femtosecond laser pulse at 800 nm was used to perpendicularly illuminate the dispersion sample. The optical power through the dispersion was monitored by detector 1 (D1) while the back-scattering light collected by the lens was monitored by detector 2 (D2). By gradually increasing the input power, we could identify the changes occurring in the transmittance and back-scattering power under different input fluences. The transmittance curve is shown in Fig. 6(b), and we can see that the transmittance peak increases as the input fluence increases up to 60 mJ/cm^2 and then becomes saturated at an incident fluence of 60~105 mJ/cm^2 and suddenly drops at 120 mJ/cm^2. At the same time, the scattering power linearly increases with the input fluence up to 105 mJ/cm^2 and then significantly increases around 120 mJ/cm^2. We found that the sudden transmittance change was caused by laser-induced microbubbles at an input fluence above 120 mJ/cm^2. On the basis of these findings, we can conclude that the sudden transmittance decrease of MoS_2 dispersion originates from the back scattering of microbubbles within the solution, which can induce the transition from saturable absorption to RSA under femtosecond laser pulse excitation. The transmittance data can be well fitted by the saturable model above, and the saturable intensity and modulation depth are inferred to be about 337.9 GW/cm^2 and 33%, respectively.

To suppress the nonlinear scattering effect that arises from laser-induced microbubbles, MoS_2 NPs were cast as a thin film on quartz plate and open-aperture Z-scan measurements were performed on it. The sample was made by spin coating MoS_2 dispersions onto a 1-mm-thick quartz plate and then drying it in an oven. The average thickness of the sample was measured to be about 10 nm. Through the performance of similar Z-scan measurements, the saturable absorption of MoS_2 film was also experimentally identified under different excitation fluence. Figure 7(a), which shows typical saturable absorption curves at different input intensities, indicates the clear dependence of the transmittance peak on the input intensity. To further ensure that the detected sample was free of optical damage, the reproducibility of the transmission curves was tested by cycling the laser fluence up and down. By either increasing the incident laser from low to high power or vice-versa, the measured nonlinear optics curves could be well reproduced at different powers.

To verify whether the quartz substrate contributes to the nonlinear optics response, pure quartz substrate without sample was used as the control, and there was no response even after irradiation at high laser power. The corresponding saturable absorption curves are shown in Fig. 7(b), from which the saturation intensity and modulation depth are determined to be 1.85 GW/cm^2 and 15.9%, respectively. Unlike the experiments with the dispersion solution,

#205894 - $15.00 USD Received 3 Feb 2014; revised 10 Mar 2014; accepted 12 Mar 2014; published 20 Mar 2014
(C) 2014 OSA

nonlinear scattering has been mitigated here, which does not allow for the emergence of the RSA effect. Consequently, we can safely conclude that the observed saturable absorption response should only originate from the intrinsic absorption in MoS_2, whereas micro bubble-induced nonlinear scattering can produce the optical limiting effect in the MoS_2 dispersion solution.

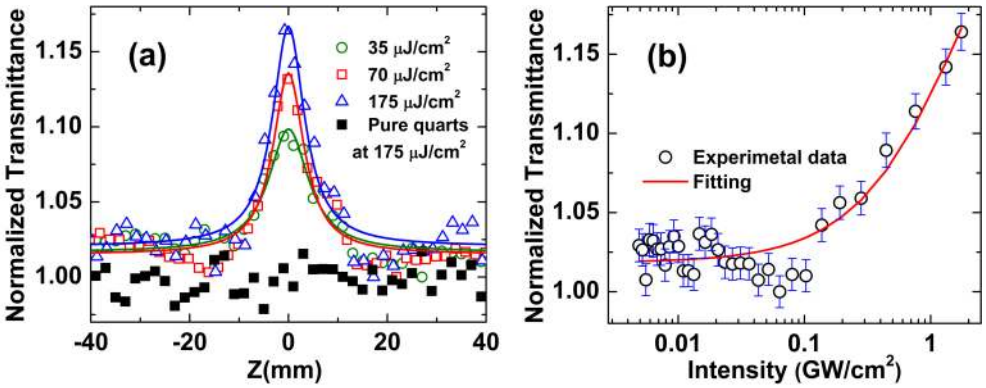

Fig. 7. (a) The open-aperture Z-scan measurement of MoS_2 NPs on quartz at different input influences at 800 nm; (b) the relation between normalized transmittance and input intensity.

To check whether the MoS_2 NPs also show saturable absorption at other wavelengths, the film sample was also measured at 1064 nm. We used a passively mode-locked ytterbium-doped fibre laser (centre wavelength: 1064 nm, repetition rate: 7 MHz and pulse duration: 0.8 ns) as the laser source. After collimation and focusing, the incident beam waist was estimated to be about 18.4 μm at the focus point. The open-aperture Z-scan technique was performed, and the saturable absorption curves were found at different input intensities, as shown in Fig. 8(a). The twin-detector method was also used to check the nonlinear absorption at different points on the sample, and we could also observe very strong saturable absorption response, as shown in Figs. 8(b) and 8(c). From the nonlinear optics curves, the saturable intensity and modulation depth are fitted to be 8.7 MW/m^2 and 4.6%, respectively. Based on both the open-aperture *Z*-scan and balanced twin-detector measurements, it can be concluded that similar to graphene, MoS_2 can act as a broadband saturable absorber in the visible to the near-infrared band.

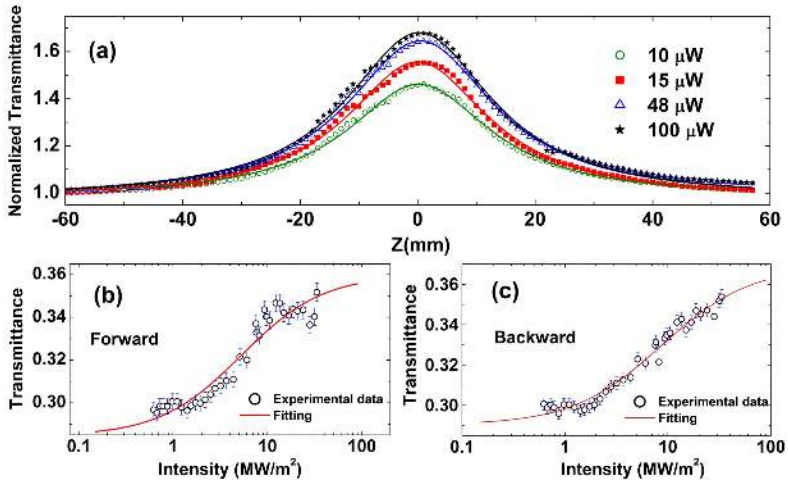

Fig. 8. (a) The open-aperture Z-scan measurement of MoS_2 NPs on quartz at different input intensities at 1064 nm. (b) and (c) The twin-detector measurement of the film sample at 1064 nm: the incident power is increased (with respect to decreased) from low (with respect to high) to high (with respect to low) intensity.

#205894 - $15.00 USD Received 3 Feb 2014; revised 10 Mar 2014; accepted 12 Mar 2014; published 20 Mar 2014
(C) 2014 OSA

4. Ultrafast photonics applications

The optical saturable absorption of MoS_2 for the passive mode locking of a fibre laser was also investigated. To make the absorber more compatible with the fibre laser cavity, the optical trapping method was used to deposit MoS_2 flakes onto the optical fibre facet. Under laser illumination, thermal convection flow and thermal diffusion can occur. These will allow for the movement of nano-particles (herein MoS_2 flake) along the temperature gradient towards the fiber surface. In the experiment, the end of the output port of a continuous wave laser at 975nm was immersed into a Dimethyl Formamide (DMF) solution of few-layer MoS_2. Polymethyl methacrylate (PMMA) solution was used to coat the fiber pigtail for protection. By controlling the pump power and deposition time, a suitable fiber pigtailed saturable absorber device can be fabricated for our fiber laser. The fibre laser cavity is schematically shown in Fig. 9. We used a piece of 0.65-m highly ytterbium-doped ðbre (YDF, LIEKKI Yb1200-4/125) with a group velocity dispersion of –20 ps^2/km as the gain medium, and a single-mode fibre with a total length of 22.4 m fibre and group velocity dispersion of –23 ps^2/km as the other fibre component. The net cavity dispersion was normal and was estimated to be –3.09 ps^2. The laser was forward pumped by a 975-nm laser diode through a 975/1060 WDM and then emitted outside the laser cavity by a 10/90 optical coupler. Unidirectional operation can be ensured by an in-cavity polarisation-independent isolator (PII-ISO). The cavity polarisation and cavity birefringence can be adjusted by the polarisation controllers to further optimise the laser mode-locking performance. The as-fabricated MoS_2 saturable absorber device was then spliced inside the laser cavity between the PC and the PII-ISO. The output laser pulse train was monitored by an oscilloscope (Tektronix TDS3054B) and a radiofrequency analyser, and the optical spectrum and pulse duration were measured by an optical spectrum analyser (Ando AQ-6317B) with a spectral resolution of 0.015 nm.

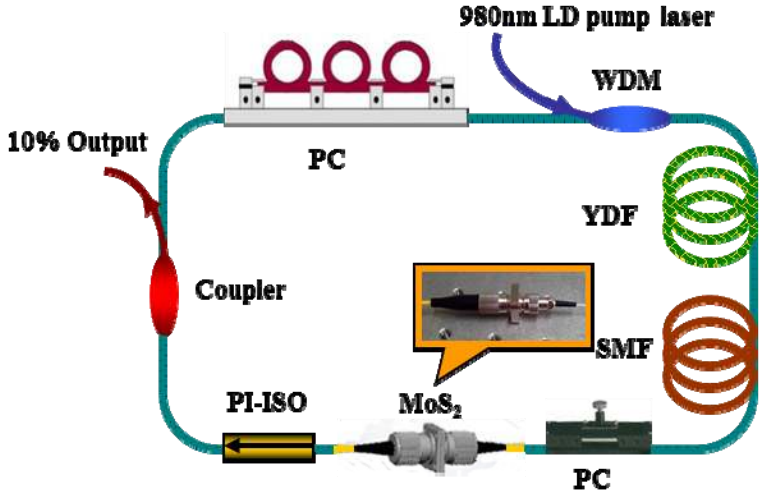

Fig. 9. Schematic of the ytterbium-doped ðbre laser passively mode locked by the MoS_2 saturable absorber. WDM (wavelength division multiplexer), YDF (ytterbium-doped fibre), PC (polarisation controller), PI-ISO (polarisation-independent isolator), SMF (single-mode fibre) and MoS_2-saturable absorber.

#205894 - $15.00 USD Received 3 Feb 2014; revised 10 Mar 2014; accepted 12 Mar 2014; published 20 Mar 2014
(C) 2014 OSA

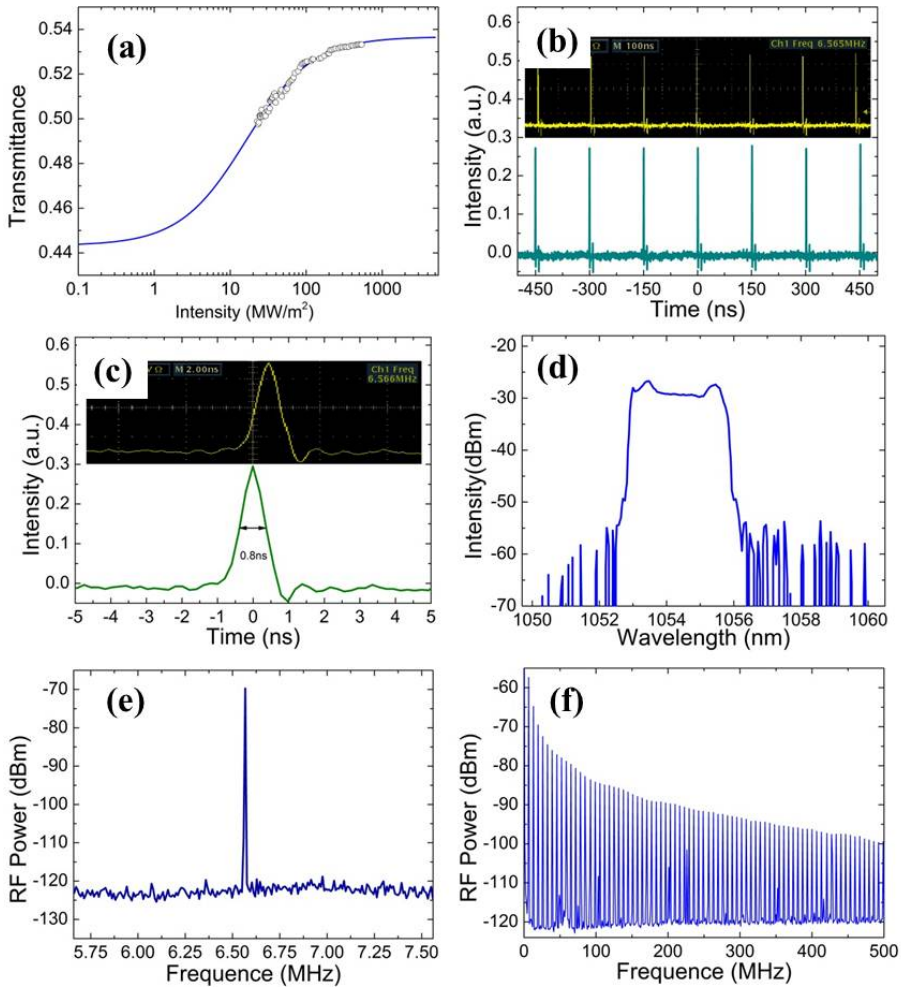

Fig. 10. The laser mode-locking performance by the MoS_2 saturable absorber: (a) the SA response fibre-pigtailed MoS_2 saturable absorber; (b) & (c) the oscilloscope tracings; (d) the optical spectrum; (e) the radiofrequency spectral profile; (f) wideband RF spectrum.

Figure 10 summarizes the nonlinear optical property of the fibre-pigtailed MoS_2 saturable absorber as well as the performance of the ytterbium-doped ðbre laser passively mode locked by the fibre-pigtailed MoS_2 saturable absorber. Figure 10(a) shows the measurement of SA curve of fibre-pigtailed MoS_2 saturable absorber. The modulation depth and the saturable intensity are inferred to be 9.3% and 15.9 MW/m^2, respectively. The mode-locking operation self-starts once the pump power exceeds 60 mW. The oscilloscope tracings of output pulses are shown in Figs. 10(b) and 10(c). Figure 10(d) shows a typical mode-locking spectrum, which has a bandwidth of 2.7 nm and a central wavelength of 1054.3 nm. Given that the total cavity dispersion is normal, it allows the generation of dissipative solitons characterised by sharp steep spectral edges in the optical spectrum [29]. Unlike the operation of conventional soliton fibre lasers, where transform-limited optical pulses (with pulse duration of hundreds of femtoseconds) can be readily generated with per-pulse energy limited at the level of tens of pico-joules, the operation of a dissipative soliton ytterbium-doped fiber laser can generate larger energy optical pulses with heavy chirp. Correspondingly, the generated optical pulse is measured to be as broad as 800 ps. However, limited by our detection system (the detector bandwidth is about 5 GHz), we are unable to probe the fine structure of the mode-locked pulses. The pulse repetition rate is about 152 nanoseconds, which corresponds to the cavity

#205894 - $15.00 USD Received 3 Feb 2014; revised 10 Mar 2014; accepted 12 Mar 2014; published 20 Mar 2014
(C) 2014 OSA

round-trip time. With continuously increasing pump power, the single-pulse operation state is maintained while the output power is increased until it reaches the maximum value of 9.3 mW. Under high pumping, the mode-locking state becomes unstable and gradually loses its stability. The corresponding radiofrequency spectrum shows that in the stable mode-locking state, the fundamental frequency has a high signal-to-noise ratio (up to 50 dB).

We note that the dissipative soliton operation of a fibre laser has been enabled by different types of saturable absorbers, including SWCNTs [30] and graphene [31–34]. The present work demonstrates the first dissipative soliton fibre laser passively mode locked by MoS_2 saturable absorber. Due to the strongly chirped feature of dissipative solitons, it can be easily amplified. After further pulse compression technology, ultrashort pulses with very large energy can be generated. The generation of dissipative solitons demonstrates that the MoS_2 saturable absorber can be used to generate large energy laser pulses.

It is worth commenting on the broadband performance of graphene and MoS_2. The broadband performance of graphene is intrinsic, due to its gapless nature. However, it is more complex in the exfoliated MoS_2 NPs sample we used due to the mixture of 1T (metallic) and 2H (semiconducting) phases present [19]. The 1T phases usually predominate in as-exfoliated samples due to doping by impurities, giving rise to similar broadband performance as graphene. If the MoS_2 can be rendered predeominantly 2H, its absorption at resonance energy will be stronger. This means that at specific wavelength that is in resonance with the band gap, we expect that MoS_2 saturable absorber can potentially give stronger saturable absorption response than graphene in view of its strong bulk-like photon absorption and exciton generation owing to Van Hove singularities.

5. Conclusion

In conclusion, we have characterised the broadband saturable absorption properties of few-layered MoS_2 from the visible band to the near-infrared band. Our measurements of the nonlinear absorption of solution-dispersed MoS_2 yielded saturation intensity and normalized modulation depth of 136.1 ± 20 GW/cm^2 and 10% at 400-nm femtosecond laser excitation and 279.6 ± 60 GW/cm^2 and 34% at 800-nm excitation, respectively. However, a higher incident laser flux leads to RSA, which arises from the laser-induced microbubbles in the solution. In the case of few-layered MoS_2 thin film, even under very high laser fluence of 100 mJ/cm^2, only saturable absorption with a saturation intensity of 1.85 GW/cm^2 and modulation depth of 15.9% is observed.

To take advantage of the saturable absorption properties of MoS_2 at the near-infrared band, we fabricated a new type of MoS_2-based optical fibre saturable absorber device that fits the mode-locking operation of an ytterbium-doped fibre laser and experimentally achieved the generation of a nanosecond dissipative soliton pulse at 1054 nm. The demonstrated pulsed laser performance includes a 3-dB spectral bandwidth of 2.7 nm and pulse duration of 800 ps, which indicates that the MoS_2 saturable absorber also possesses mode-locking ability that is at least comparable with that of conventional saturable absorbers such as graphene.

Acknowledgments

This work is partially supported by the National 973 Program of China (Grant No. 2012CB315701). K.P.L. offers thanks for the MOE Tier 1 grant “Two dimensional crystals as platforms for optoelectronics (R-143-000-556-112)” and also the NRF-CRP project “Novel 2D materials with tailored properties: beyond graphene (R-144-000-295-281)”. H. Z. offers thanks for the MOE grant (Grant No. NCET 11-0135) and National Natural Science Fund (Grant No. 61222505). The authors would like to thank Dr. Xiang Qi at Xiangtan University for providing the Raman characterization data.